# $BiF_3$ Incorporation in Na/Ba Mixed Network Modifier Fluoride-Phosphate Glasses: Structural Studies by Solid State NMR and Raman Spectroscopies

Gustavo Galleani[a], Henrik Bradtmüller[b], Hssen Fares[c], Silvia Helena Santagneli[c], Marcelo Nalin[c] and Hellmut Eckert[a,b]

[a] *São Carlos Institute of Physics – São Paulo University – USP, Avenida Trabalhador Saocarlense 400, São Carlos-SP, 13566-590, Brazil*

[b] *Institut für Physikalische Chemie, Westfälische Wilhelms-Universität Münster, Corrensstr. 30, D-48149 Münster, Germany*

[c] *Institute of Chemistry, São Paulo State University-UNESP, Araraquara-SP, Brazil*

# Abstract

Bismuth-containing rare-earth co-doped fluoride phosphate glasses are promising materials for super-broadband near-infrared (NIR) emission with potential applications in optical amplification. To elucidate their structural organization this contribution develops a comprehensive multinuclear solid-state single and $^{31}P/^{19}F$ double resonance NMR strategy, applied to glasses in the system $(BiF_3)_y(50NaPO_3–20Ba(PO_3)_2–20NaF–10BaF_2)_{100–y}$ ($y$ = 0, 5, 10, 20, 30, 40). To separately assess the influence of bismuth and fluorine constituents on the network structure, an additional set of $(NaPO_3)_{50–2x}(Ba(PO_3)_2)_{20–x}(NaF)_{20+2x}(BaF_2)_{10–x}$ ($x$ = 0, 2.5, 5.0, 7.5) glasses was also investigated. Introduction of alkali fluoride ions into phosphate glasses is shown to follow a new network modification scheme involving depolymerization of polyphosphate chains under the formation of F-bonded fluorophosphate units. However, a significant part of the fluoride stays separate, interacting exclusively with metal ion species. $^{23}Na$ MAS and $^{23}Na\{^{31}P\}$ double resonance NMR results are consistent with a local sodium ion environment dominated by phosphate ions in the Bi-free system, whereas in the $BiF_3$-containing glasses, the successive reduction of the dipolar second moment $M_{2(Na-P)}$ with increasing $BiF_3$ content reflects the expected dilution effect, accompanied by increasing competition of the fluoride ions for ligation with the $Na^+$ ions.

# 1. INTRODUCTION

Oxyfluoride glasses containing heavy metal oxides and fluorides are receiving increasing research attention and technological use due to their widespread applications in optics and as opto-electronic devices. The incorporation of $Bi_2O_3$ and $BiF_3$ into these glasses is of particular interest because of their usually wide transmission window in the IR and the increased refractive index, important for non linear optical properties. In addition, these glasses offer new and interesting optical properties based on Bi-specific luminescence in the visible and broadband luminescence in the NIR over the 1000 to 2000 nm region. [1–5]

Glasses containing bismuth have been proposed in applications such as broadband high gain optical amplifiers,[6] tunable lasers,[7] and fibers.[8,9] $Bi^{3+}$ ions can also function as sensitizers to increase the efficiency of energy transfer to rare earth ions for specific photovoltaic applications.[10] Numerous bismuth-containing systems have been prepared on germanate[11], silicate[12], phosphate[4], borate[13] and oxyfluoride[14] glass bases and characterized with respect to their physical properties .

Recently, fluorophosphate (FP) glasses have attracted much attention as optical media for luminescence-active ions. They offer the prospect of combining the favorable mechanical properties of oxide glasses, with oxygen playing the role of stabilizing the vitreous state, with the desirable optical properties (low-phonon rare-earth environments) of fluoride glass matrices.[13,15–19] Past studies have shown that the mechanical properties and emission characteristics of FP glasses can be sensitively tuned by the fluoride/phosphate ratio of the batch composition and much work was done on alkali[20,21], aluminum[17–19] and indium[22] fluorophosphate glasses. Therefore, understanding the structural role of the $BiF_3$ component is of great interest.

Nuclear magnetic resonance is a powerful tool for the structural characterization of glasses.[23-27] For fluorophosphate glasses in particular, the combination of magic-angle spinning with more advanced dipolar NMR methodology has provided significant information regarding the short- and medium range order in a number of fluorophosphate glass systems.[17-19, 22, 28-30] In this paper, we report a detailed study on the incorporation of $BiF_3$ in the $(NaPO_3)(Ba(PO_3)_2)(NaF)(BaF_2)$ glass system. To be able to characterize the effects of bismuth and fluoride incorporation separately, a second set of Bi-free glasses

has been examined in which the fluoride/phosphate ratio has been varied systematically, without altering the cation composition. Based on a detailed characterization of these glasses by Raman spectroscopy and one and two-dimensional solid-state NMR techniques, we obtain structual insights into the speciation and distribution of the fluoride component and propose a model describing its role in the structural transformation of the phosphate network.

# EXPERIMENTAL

### Sample Preparation and Characterization

To separately study the effects of the phosphate/fluoride ratio and the Bi content on the functional and structural properties of the glasses of interest, two glass series with batch chemical compositions of i) $(NaPO_3)_{50-2x}(Ba(PO_3)_2)_{20-x}(NaF)_{20+2x}(BaF_2)_{10-x}$ ($x$ = 0, 2.5, 5.0, 7.5; PFG-x series) and ii) $(BiF_3)_y(50NaPO_3–20Ba(PO_3)_2–20NaF–10BaF_2)_{100-y}$ ($y$ = 0, 5, 10, 20, 30, 40, PFG-yBi series) were examined, see Table 1. Transparent colorless specimens were prepared in 10 g batches via the standard melt-quenching technique. Raw materials were $BaF_2$ (Sigma-Aldrich, 99%), NaF (Sigma-Aldrich, 99.9%), sodium metaphosphate ($NaPO_3$, Alfa Aesar, 99%) and barium metaphosphate ($Ba(PO_3)_2$, Sigma-Aldrich, 99%). $BiF_3$ was synthesized by heating $Bi_2O_3$ (Strem Chemicals, 99.9%) with an excess of ammonium bifluoride ($NH_4HF_2$, Alfa Aesar, 95%) in an open platinum crucible at 400 °C for 2 h. Afterwards, the powder was heated to 600 °C for 60 min to ensure complete elimination of $NH_3$ and HF from the decomposition of ammonium bifluoride. The purity of this material was ensured by X-ray powder diffraction (JCPDS 01-070-0549).[23] Approximately 10 g batches of the starting materials were finely ground in an agate mortar and then melted at 900 °C for 20 min in a Pt/Au (Vectra, 98/2 mol%) crucible in ambient atmosphere. Subsequently, the glass melt was poured into a rectangular steel mold preheated to 200 °C. After a holding time of 3 h, the material was cooled to room temperature with a cooling rate of 5 °C/min, in order to reduce residual internal stresses. The characteristic temperatures of the glasses were measured using a TA Instruments 2910 differential scanning calorimeter. Typically, 15 mg of a sample

were sealed within aluminum pans and heated at a rate of 10 °C/min under $N_2$ atmosphere. The errors associated with the glass transition temperature, $T_g$ and the onset temperature of crystallization, $T_x$ were ± 2 °C.

Table. 1. Glass compositions, glass transition onset temperatures $T_g$ and crystallization peak temperatures $T_x$ of the samples under study.

| Composition | $NaPO_3$ | $Ba(PO_3)_2$ | NaF | $BaF_2$ | $BiF_3$ | P/F | $T_g$ / $^0$C | $T_x$ / $^0$C |
|---|---|---|---|---|---|---|---|---|
| {*x*,*y*} = 0 | 50 | 20 | 20 | 10 | - | 2.3 | 289 | 397 |
| *x* = 2.5 | 45 | 17.5 | 25 | 12.5 | - | 1.7 | - | - |
| *x* = 5.0 | 40 | 15 | 30 | 15 | - | 1.2 | - | - |
| *x* = 7.5 | 35 | 12.5 | 35 | 17.5 | - | 0.9 | - | - |
| *y* = 5 | 47.5 | 19 | 19 | 9.5 | 5 | 1.6 | 271 | 386 |
| *y* = 10 | 45 | 18 | 18 | 9 | 10 | 1.2 | 250 | 371 |
| *y* = 20 | 40 | 16 | 16 | 8 | 20 | 0.8 | 248 | 352 |
| *y* = 30 | 35 | 14 | 14 | 7 | 30 | 0.5 | 242 | 335 |
| *y* = 40 | 30 | 12 | 12 | 6 | 40 | 0.4 | 242 | 323 |

**Solid-state NMR studies**

Single resonance multinuclear magic-angle spinning (MAS) NMR experiments were carried out at 5.7, 9.4, and 14.1 T using an Agilent DD2 spectrometer interfaced with a 5.7 T magnet, Bruker Avance III HD and DSX 400 spectrometers and a Bruker Avance Neo 600 MHz spectrometer. $^{19}$F MAS NMR spectra were measured at 5.7 T, in 1.6 mm rotors spinning around the magic-angle at 40.0 kHz, using a rotor-synchronized Hahn-Echo sequence with an interpulse delay of 4 rotor cycles for removal of any probe background signal. Different evolution times (from 2 to 12 rotor cycles) were tested and it was found that the values used in the experiments influence the relative intensities of the resolved spectral components, indicating different spin-spin relaxation times for them. 90 ° pulses of 1.65 μs length and relaxation delays of 20 s were used. Chemical shifts are reported relative to $CFCl_3$ (0 ppm) using solid $AlF_3$ (−172 ppm) as a secondary reference. $^{19}$F{$^{31}$P} REDOR measurements were carried out in a 3.2 mm probe and a magic-angle spinning frequency of 25.0 kHz, using the standard Gullion-Schaefer sequence[24] with correction by the compensation method.[25] In these experiments, the π pulse length was 4.0 μs for both isotopes and the π-pulses applied to the non-observed nuclus ($^{31}$P) were phase cycled according to the XY-4 scheme.[26]

$^{31}$P MAS NMR spectra were recorded at 5.7 T and a magic-angle spinning frequency of 12 kHz using π/2 pulses of 3.3 μs length and a relaxation delay of 300 s.

Chemical shifts were referenced against 85% $H_3PO_4$ (0 ppm). Peak assignments were supported by a $^{31}P\{^{19}F\}$REDOR experiment, carried out on a representative sample under the following conditions: magic-angle spinning frequency of 15 kHz, 180° pulse lengths of respectively 12.8 and 9.8 μs for $^{31}P$ and $^{19}F$, relaxation delay of 350 s. $^{31}P$ J-resolved NMR experiments were done using the rotor-synchronized Hahn spin echo sequence including a z-filter and using a 32-step phase cycle.[27] The π/2 pulse lengths were around 1.5 μs, and a z-filter delay of one rotor period was used at a MAS frequency of 14 kHz. $^{23}Na$ MAS NMR spectra were recorded at 9.4 T at a spinning speed of 12.0 kHz using short pulses of 1.0 μs length and a relaxation delay of 2 s. Chemical shifts are reported relative to a 1 mol $L^{-1}$ NaCl aqueous solution (0 ppm). $^{23}Na\{^{31}P\}$ Rotational Echo Double Resonance (REDOR) experiments were done at 9.4 T, at a MAS frequency of 14.0 kHz using the sequence of Gullion and Schaefer.[24] The optimum π pulse lengths for the decoupling channel were obtained by maximizing the REDOR difference signal $\Delta S$ at a fixed dephasing time. Optimum values were 4.2 and 6.0 μs for $^{23}Na$, and $^{31}P$, respectively. XY-4 phase cycling was used for the $^{31}P$ recoupling π-pulses. Normalized difference signal intensities for each phosphate site, $(\Delta S/S_0$, corresponding to the signal amplitudes without ($S_0$) and with ($S$)) were obtained from signal deconvolution with the DMfit software using Gaussian functions,[28] and were plotted as a function of dipolar mixing time $NT_r$. In all the REDOR experiments approximate second moments $M_{2(S\text{-}I)}$ were obtained by applying a parabolic fit to the REDOR data within the range $\Delta S/S_0 \leq 0.2$, according to the expression[29]

$$\frac{\Delta S}{S_0} = \frac{4}{3\pi^2}(NT_r)^2 \, f \, M_{2(\mathrm{S-I})}. \qquad (1)$$

In this expression, $NT_r$ is the number of rotor cycles multiplied by the length of the rotor period, defining the dipolar mixing time, and $f$ is a scaling factor determined by comparing the experimentally measured $M_2$ value on a crystalline model compound with the theoretically expected value calculated from the internuclear distances of its crystal structure. The value for $f$ is a number between zero and one and reflects experimental imperfections such as resonance offsets, π-pulse missets, and effects due to non-negligible pulse lengths in comparison with the duration of the rotor cycle. The second moment values, in turn, can be calculated from internuclear distance distributions using the van Vleck expression[30]

$$M_{2(\mathrm{S-I})} = \frac{4}{15}\left(\frac{\mu_0}{4\pi}\right)^2 I(I+1)\gamma_I^2\gamma_S^2\hbar^2 N^{-1}\sum_S \frac{1}{r_{IS}^6}. \qquad (2)$$

This equation was used to calibrate the second moment values obtained from the REDOR experiments on the crystalline model compounds $Na_2PO_3F$ and $NaPO_3$.

# RESULTS AND DISCUSSION

### Physical Properties

All glasses are visually transparent and homogenous. The PFG-x glass series are highly hygroscopic and not stable under ambient conditions. Therefore, the glasses were stored in a dry glove box after their preparation and were only removed for structural characterization. In contrast, all of the Bi-containing glasses (PFG-y glass series) are more stable towards ambient atmospheric conditions. As indicated by Table 1, the addition of up to 20% $BiF_3$ leads to a significant and monotonic decrease in $T_g$ values. Any $BiF_3$ addition beyond this point shows no further changes in $T_g$ but only decreases the glass stability parameter $T_x$-$T_g$.

### Raman scattering.

Figure 1a and b shows the Raman spectra of the two glass series. Overall, the spectra are very similar in both series and show comparable trends. Three strong bands can be observed at ~1140, 1100, and 1010 $cm^{-1}$, attributable to the $PO_2$ stretching modes of metaphosphate groups, the $PO_3$ symmetric stretching modes of $P_2(O,F)_7$ dimers, and the $PO_4$ and/or $PO_3F$ units of isolated ortho- or fluorophosphate units. In addition, the shoulder at ~900 $cm^{-1}$ suggests the presence of direct P-F bonding and the band observed at 750 $cm^{-1}$ can thus be attributed to the P-O-P stretching mode involving dimeric groups. With increasing F/P ratio (respectively increasing *x* and *y* in the glass composition), the intensity of the 1010 $cm^{-1}$ band increases at the expense of the of the higher-frequency bands. Alongside, there is a decrease in the peak near 750 $cm^{-1}$, accompanied by a small high-frequency shift. This shift is typically observed in binary alkali phosphate glasses, reflecting a transformation from metaphosphate ($Q^2$) to pyrophosphate ($Q^1$) units.[31] All of these findings consistently indicate a successive decrease in the connectivity of the glass network as the fluoride content increases in the PFG-x series and in the PFG-yBi series. At lower frequency, the band at 540 $cm^{-1}$ is assigned to NaF.[32] However, in the

PFG-yBi series a new band appears centered at 440 $cm^{-1}$ and increases with increasing $BiF_3$ content. This band is commonly observed in bismuth containing fluoride glasses[33] and lies within the range of the vibrational modes observed for crystalline $BiF_3$.[34]

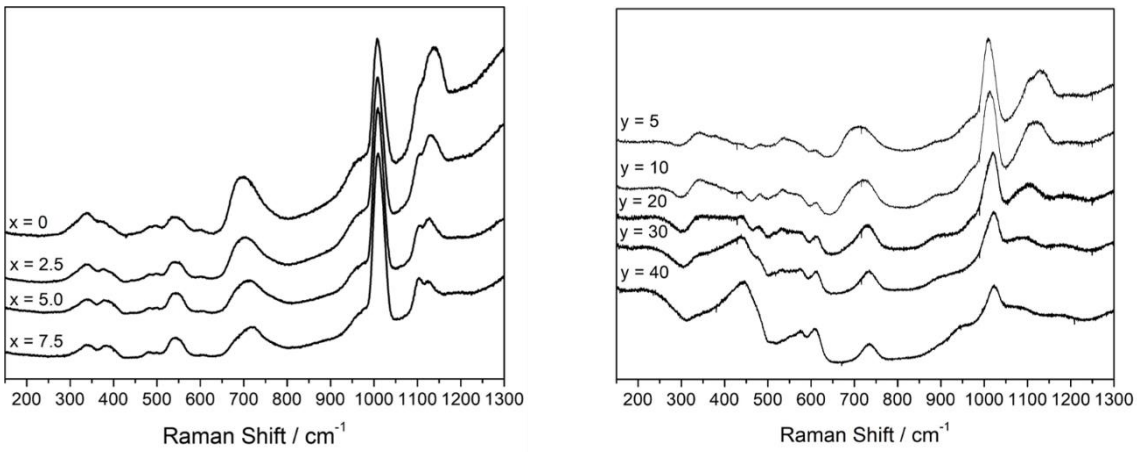


**Figure 1.** Raman spectra of the PFG-x (left) and PFG-yBi (right) glass series.

## $^{19}F$ MAS NMR and $^{19}F\{^{31}P\}$ REDOR.

Figure 2 shows the $^{19}F$ MAS NMR spectra of both glass series. The use of rotor-synchronized spin echo experiments was found to be mandatory to effectively suppress the significant probe background signal. In the spectra of the $BiF_3$-free PFG-x glasses, four principal contributions can be identified, with isotropic chemical shift values near -39, -69, -140 and -226 ppm. These four components also form the basis for the deconvolutions made for the $^{19}F$ NMR spectra of the $BiF_3$ containing glasses (PFG-y series) which, however, feature additional species, resulting in considerable spectral overlap. Table 2 summarizes the spectroscopic parameters obtained from the spectral deconvolution into the respective components. Note that the area ratios only reflect the actual population ratios if spin-spin relaxation occurring between the initial 90° pulse and the elapsed time until echo aqcuisition is identical for the all present fluorine species. Figure 3 examines this question for a representative sample containing 30 mol% $BiF_3$, by measuring the normalized $^{19}F$ spin echo intensities as a function of the number of rotor cycles for the four above-mentioned components. Clearly the signal at -68.5 ppm decays significantly more slowly with increasing number of rotor periods than the fluoride species represented by the other three deconvolution components. Owing to this difference, the area fraction of the fluoride species at -68.5 ppm may be significantly over-estimated in the lineshape deconvolution. Corrections of these area fractions via

back-projection of the data of Figure 3 are possible in principle, but only with a large degree of experimental uncertainty, because the number of available data points is rather limited. In Figure 3c we show the result of such an exemplary analysis, by fitting the data to exponential decays, producing apparent $T_2$ values of 0.4, 0.2, 0.2, and 0.25 ms, for the signals at -68.5, -133, -54, and -103 ppm, respectively. Estimated populations of these four species, based on exponential back-projections have been included in Table 2 for this composition, suggesting that the -68.5 ppm species comprises only 37% of the F-species compared to the value of 46% obtained by direct deconvolution of the Fourier-transformed echo. The most probable origin of the different $T_2$ values are different strengths of the homo-nuclear $^{19}F$-$^{19}F$ dipole-dipole interactions. Particularly rapid decays are expected in the case of clustered fluoride ion arrangements, which result in very strong dipolar interactions. $^{19}F$ MAS NMR peak assignments were further corroborated by $^{19}F\{^{31}P\}$ REDOR experiments, shown in Figure 4. Part c) of this figure shows the Fourier transforms of $S$, $S_0$, and $\Delta S$ measured in a REDOR experiment on glass $y = 10$ for a dipolar mixing time of 0.4 ms. From this result it is obvious that under the conditions measured (20.0 kHz MAS) reliable REDOR curves can only be obtained for the P-bonded F species (peak near 69 ppm) and for the Na-bonded F species (peak near -222 ppm), whereas for the other signal components the rotor-synchronized reference signal $S_0$ decays too rapidly. Note that for this particular spectral component $^{31}P$ dipolar recoupling over 8 rotor cycles (0.4 ms) leads to the complete disappearance of the signal, reflecting the expected strong $^{31}P$-$^{19}F$ dipole-dipole interaction, also observed in the $Na_2PO_3F$ model compound. Thus, the resonance at 69 ppm can be unambiguously assigned to P-bonded fluorophosphate species, which is consistent with previous studies.

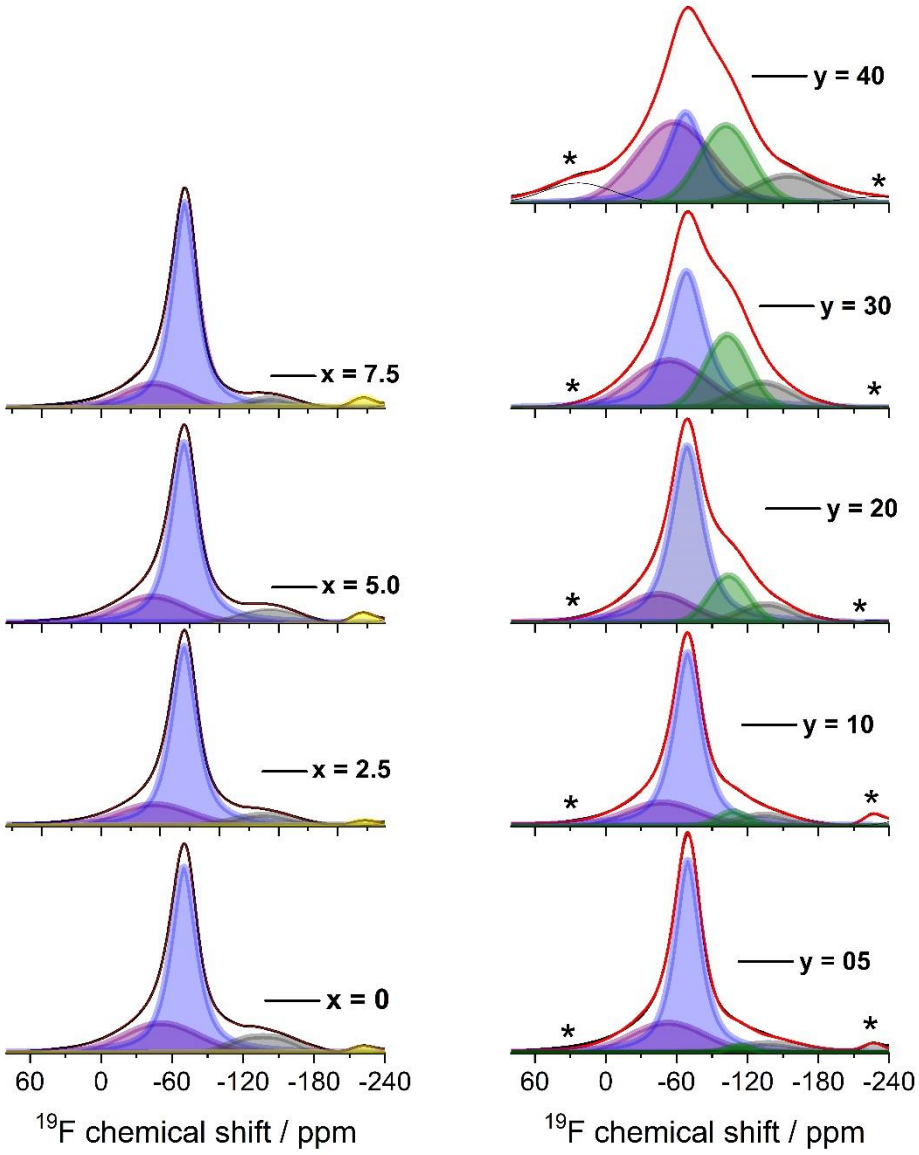


**Figure 2.** $^{19}$F MAS NMR spectra of the PFG-x and PFG-yBi glass series under study, showing the proposed deconvolution model into four Gaussian lineshape components.

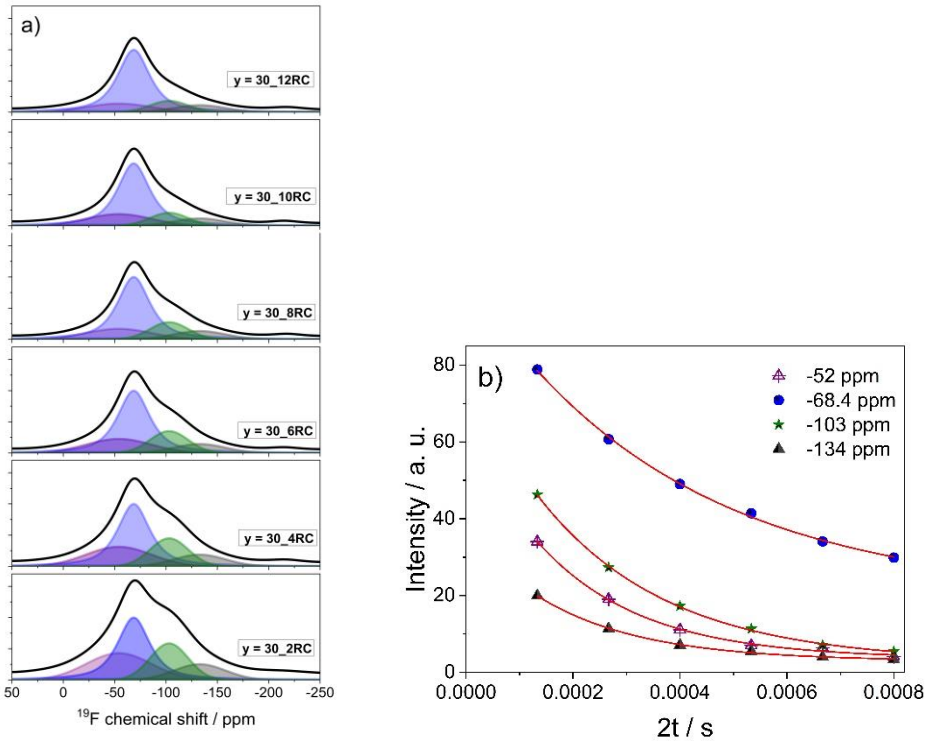


**Figure 3.** a) $^{19}$F MAS NMR spectra obtained on the sample $y = 30$, recorded as rotor synchronized spin echoes with different numbers of rotor cycles. b) Plot of echo intensities (in arbitrary units) as functions of evolution evolution time $NT_r$ and fits using an exponential function, producing the spin-spin relaxation times mentioned in the text.

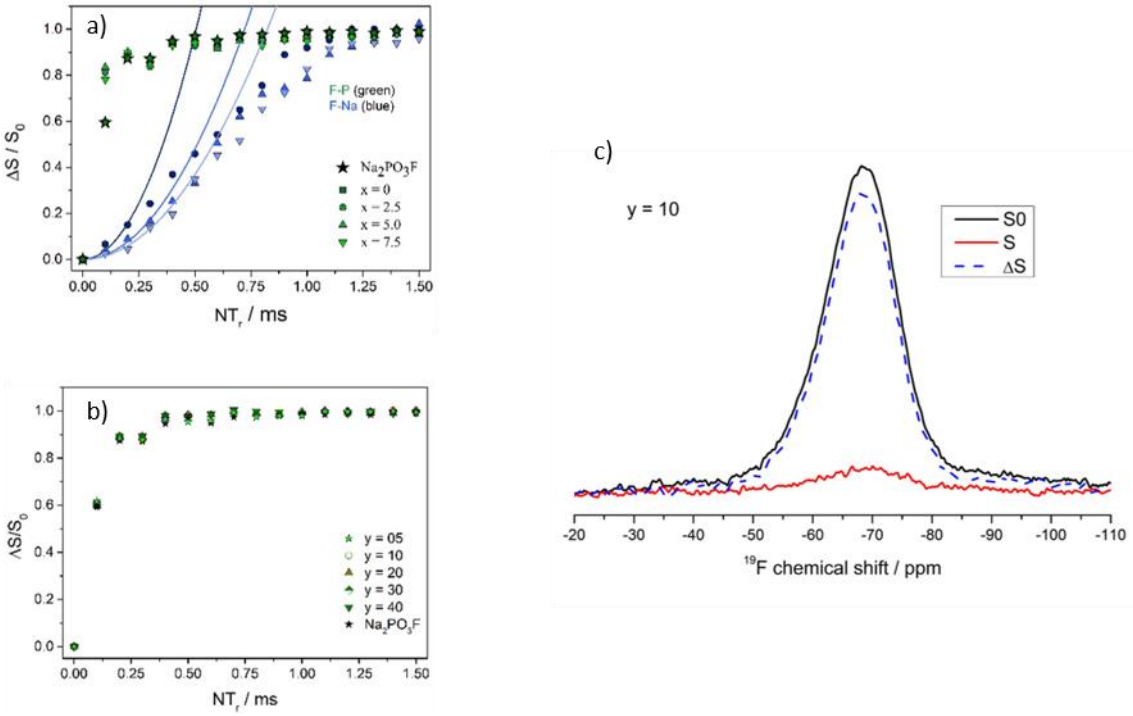


**Figure 4.** Left: $^{19}$F{$^{31}$P} REDOR experiments conducted on the glass series PFG-x (a)) and PFG-yBi (b)). Under the conditions measured (20 kHz MAS) reliable REDOR data sets could only be obtained for the P-bonded F species (peak near -69 ppm) and for the Na-bonded F species (in the

case of the PFG-yBi series, peak near -222 ppm), whereas for the other signal components the reference signal $S_0$ decayed too rapidly (as evident from the Fourier Transform shown in c)). c) Fourier Transforms of the signals $S_0$, $S$, and $\Delta S$, on glass $y = 10$, for a dipolar mixing time of 0.4 ms, indicating very strong dipolar coupling, consistent with the situation for the P-bonded F species.

**Table 2.** $^{19}$F MAS NMR lineshape deconvolution parameters for the studied glasses. Estimated errors are ±0.5 ppm for chemical shifts, ±2% for areas.

| Glass composition | F-P | | | | F-Na | | F-Ba | | F-Bi | |
|---|---|---|---|---|---|---|---|---|---|---|
| | $\delta_{iso}$ (ppm) | Area (%) | $\delta_{iso}$ (ppm) | Area (%) | $\delta_{iso}$ (ppm) | Area (%) | $\delta_{iso}$ (ppm) | Area (%) | $\delta_{iso}$ (ppm) | Area (%) |
| x = 0 | -69.2 | 68.7 | -140.0 | 8.1 | -226.4 | 1.3 | -38.9 | 21.9 | - | - |
| x = 2.5 | -70.3 | 73.3 | -137.3 | 7.2 | -222.9 | 1.4 | -45.4 | 18.1 | - | - |
| x = 5.0 | -70.1 | 72.0 | -142.0 | 8.5 | -222.2 | 4.0 | -43.7 | 15.4 | - | - |
| x = 7.5 | -70.6 | 75.3 | -144.0 | 4.9 | -222.0 | 3.1 | -45.1 | 16.8 | - | - |
| y = 5 | -69.6 | 77.4 | -131.7 | 6.7 | -222.1 | 1.4 | -44.1 | 12.5 | -126.1 | 2.0 |
| y = 10 | -69.4 | 69.3 | -134.6 | 5.8 | -227.1 | 2.7 | -48.2 | 17.7 | -124.7 | 4.5 |
| y = 20 | -69.0 | 61.6 | -135.9 | 8.1 | - | - | -45.0 | 15.4 | -121.3 | 14.9 |
| y = 30 | -68.5 | 45.9/36.5* | -132.8 | 18.1/13.0* | - | - | -54.0 | 20.8/22.8* | -120.0 | 15.2/27.7* |
| y = 40 | -67.7 | 47.3 | -137.5 | 3.5 | - | - | -58.1 | 12.8 | -118.8 | 36.5 |

*back-projected signal fractions from echo experiments with different numbers of rotor cycles.

### $^{31}$P MAS NMR and $^{31}$P{$^{19}$F} REDOR

Figure 5 shows results from single pulse $^{31}$P MAS NMR experiments for the set of fluorophosphate glasses with different F/P ratios studied in this work. In all the spectra, three distinct contributions can be observed: i) in the range from -15 to -17.0 ppm, ii) in the range -1.0 to -5.0 ppm, and iii) in the range 2.2 to 6.7 ppm. These contributions can be assigned to $Q^2$, $Q^1$, and $Q^0$ units, respectively, and their precise locations depend on the composition in a systematic fashion. With increasing $BiF_3$ content the $Q^0$ and $Q^1$ signals shift towards lower frequencies, presumably reflecting an increasing extent of interaction of these anionic phosphate species with the $Bi^{3+}$ ions.

The assignment of the resonance near -5 ppm to a $Q^1$ species in the samples containing 30 and 40 mole % $BiF_3$ was further confirmed by proving the existence of P-O-P connectivity via 2D J-resolved NMR spectroscopy, see Figure 6. The experiment shows a doublet characterized by an indirect spin-spin coupling constant $^2J(^{31}\text{P-O-}^{31}\text{P})$ near 20-

25 Hz in the second dimension, whereas the signal around 2.5 ppm yields a singlet representing the $Q^0$ unit.

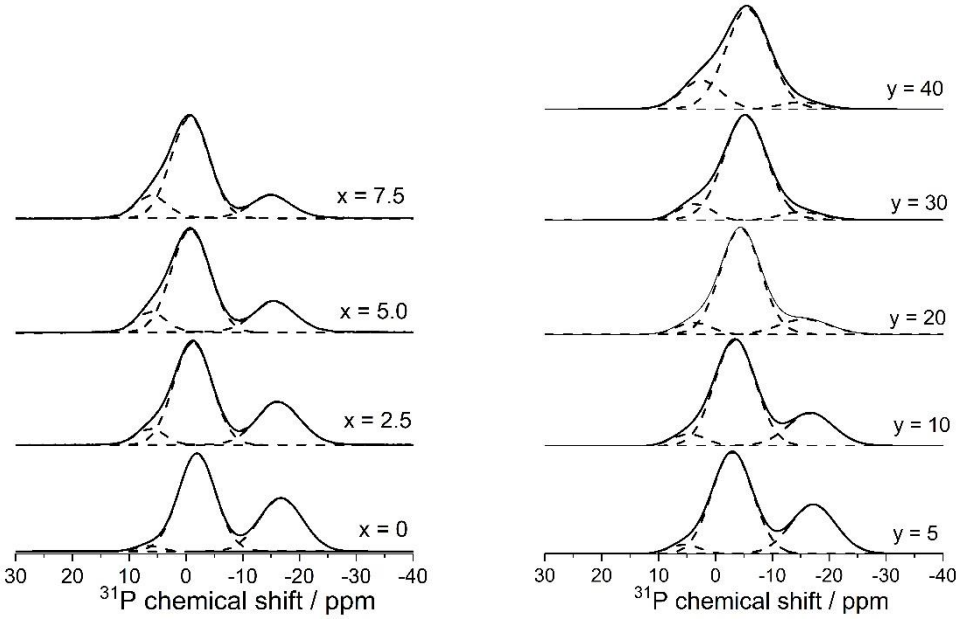


**Figure 5:** $^{31}$P MAS NMR spectra of the PFG-x and PFG-yBi glass series under study.

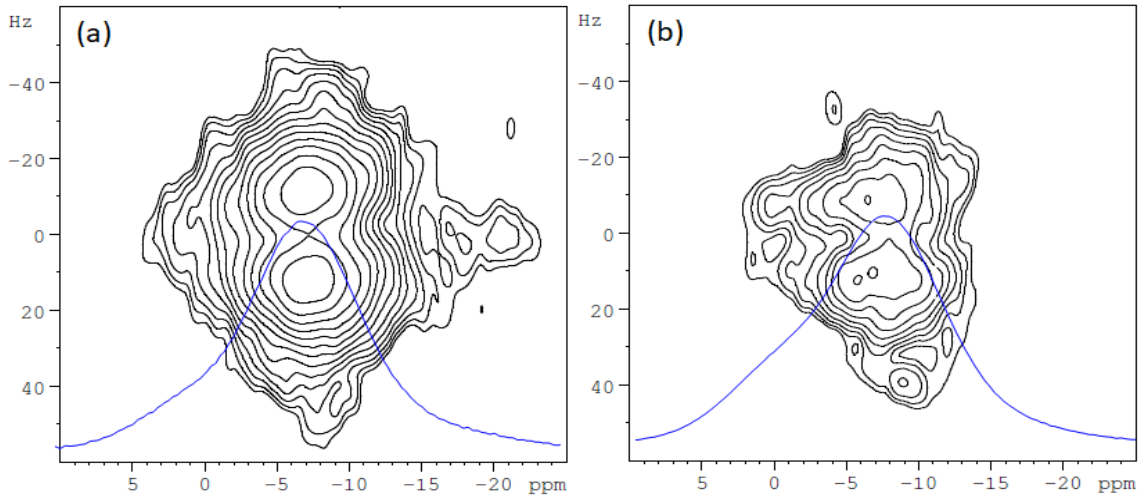


**Figure 6**. 2D J-resolved spectra of the (a) $y = 30$ and (b) $y = 40$ glass samples.

The most striking feature of Figure 5 is the systematic change in the $Q^n$ speciation with increasing fluoride content. In both series, the phosphate network becomes increasingly less polymerized, as $Q^2$ units are successively converted to $Q^1$ and further to $Q^0$ units. However, the $Q^1$ species remain dominant up to the highest fluoride contents. Table 3

summarizes these speciations. Based on those numbers, the average number of bridging oxygen atoms, <BO>, per phosphate unit are calculated, see Table 4. In

**Table 3:** Deconvolution of the $^{31}$P MAS NMR spectra of the PFG-x and PFG-yBi glass series under study. Estimated errors are ±0.5 ppm for chemical shifts, ±2% for areas.

| Sample | $Q^{(0)}$ | | $Q^{(1)}$ | | $Q^{(2)}$ | |
|---|---|---|---|---|---|---|
| | $\delta_{iso}$ (ppm) | Area (%) | $\delta_{iso}$ (ppm) | Area (%) | $\delta_{iso}$ (ppm) | Area (%) |
| x = 0 | 6.7 | 2 | -1.9 | 57 | -16.7 | 41 |
| x = 2.5 | 6.3 | 7 | -1.2 | 62 | -16.3 | 31 |
| x = 5.0 | 6.2 | 11 | -0.8 | 66 | -15.6 | 23 |
| x = 7.5 | 6.0 | 14 | -0.7 | 68 | -15.0 | 18 |
| y = 5 | 5.6 | 5 | -3.0 | 58 | -17.2 | 37 |
| y = 10 | 4.7 | 7 | -3.9 | 66 | -16.7 | 27 |
| y = 20 | 3.8 | 8 | -4.4 | 77 | -15.6 | 15 |
| y = 30 | 3.6 | 9 | -5.2 | 84 | -15.1 | 7 |
| y = 40 | 2.5 | 21 | -5.7 | 74 | -14.9 | 5 |

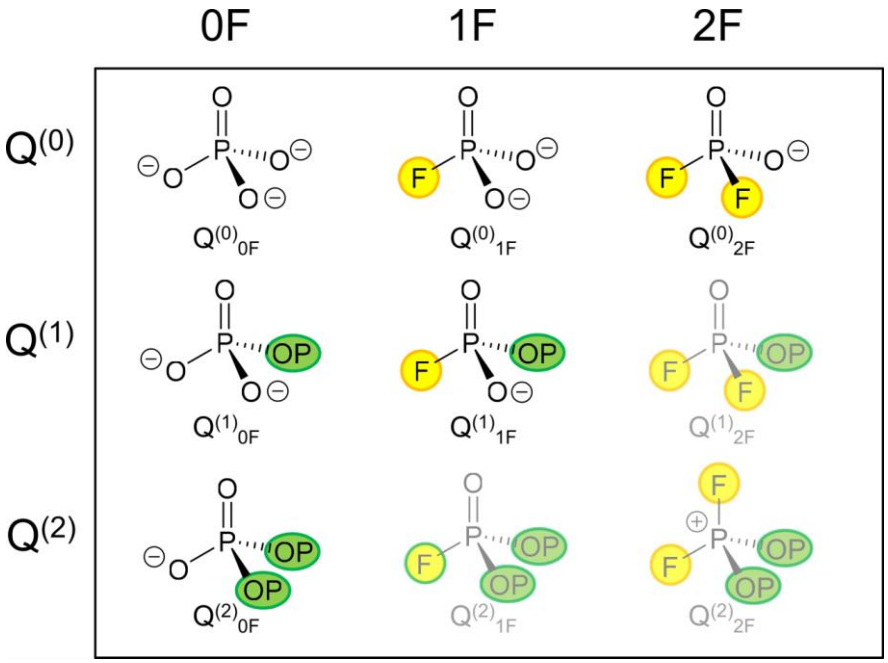


**Figure 7**: Structures of various possible network-forming units occurring in the studied glasses. Uncharged or cationic species that are less likely to occur are shown in pale colors.

both series, the successive depolymerization of the network is documented by the monotonic decrease of <BO> with increasing fluoride content.

For a structural interpretation of these results we refer to Figure 7, which illustrates up to nine possible structural units that might arise from the depolymerization of the $Q^2$ chains dominating the structure of the parent $NaPO_3$-$Ba(PO_3)_2$ glasses by adding the fluoride components. These possible depolymerization reactions may be written as follows:

$$2\{P(O)_2O_{2/2}\}^- + F^- \rightarrow \{F\text{-}P(O)_2O_{1/2}\}^- + \{P(O)_3O_{1/2}\}^{2-} \quad (1)$$

$$2\ P(O)_3O_{1/2}\}^{2-} + F^- \rightarrow \{F\text{-}P(O)_3\}^{2-} + PO_4^{3-} \quad (2)$$

$$\{F\text{-}P(O)_2O_{1/2}\}^- + \{P(O)_3O_{1/2}\}^{2-} + F^- \rightarrow 2\ \{F\text{-}P(O)_3\}^{2-} \quad (3)$$

$$2\ \{F\text{-}P(O)_2O_{1/2}\}^- + F^- \rightarrow FPO_3^{2-} + \{F_2P(O)_2\}^- \quad (4)$$

In short hand notation, equations (1) to (4) may be written as:

$$2Q^2 + F \rightarrow Q^1{}_{1F} + Q^1$$

$$2Q^1 + F \rightarrow Q^0{}_{1F} + Q^0$$

$$Q^1{}_{1F} + Q^1 + F \rightarrow 2\ Q^0{}_F$$

$$2Q^1{}_F + F \rightarrow Q^0{}_{1F} + Q^0{}_{2F}$$

Expression (1) describes the conversion of two $Q^2$ units into two $Q^1$ units by reaction with one $F^-$ ion. The P-O-P linkage is broken, resulting in one $Q^1$ unit having a P-F bond, and a second, regular $Q^1$ unit. Likewise, it takes one F species to convert two $Q^1$ units into two $Q^0$ units (expressions (2)-(4)), resulting in $Q^0$ species bonded to zero to two F atoms. While the chemical shift ranges of the non-F-bonded $Q^0$, $Q^1$, and $Q^2$ units are well-known, there are only few studies on the $^{31}P$ chemical shifts of the potential fluoride-bonded units $Q^0{}_{1F}$, $Q^0{}_{2F}$, and $Q^1{}_{1F}$.[35–37] The isotropic chemical shift values reported for $Na_2PO_3F$, which represents a $Q^0{}_{1F}$ unit, range from -0.8 ppm (in solution) to +5.9 ppm in the solid state, whereas for barium flurophosphate, $BaPO_3F$, the reported shift is -2.4 ppm. Further insights are obtained from $^{31}P\{^{19}F\}$ REDOR data, conducted on a representative sample containing 10% $BiF_3$, see Figure 8. In this experiment F-bonded phosphate species are expected to lead to very rapid dephasing, as the short P-F distance results in a very strong $^{31}P$-$^{19}F$ dipole-dipole interaction. Simulations show that complete REDOR dephasing of the $^{31}P$ spins would already occur over the time period of two rotor cycles (100 µs at the spinning frequency of 20 kHz used in our experiments). Indeed, Figure 7 confirms an intense REDOR effect for the signals near 2 ppm and -5 ppm (generally attributed to $Q^0$ and $Q^1$ units) at this rather short evolution time, whereas the effect is significantly weaker for the spins giving rise to the signal near -17 ppm. Based on this result we conclude that the $Q^0{}_{1F}$ (and possibly the $Q^0{}_{2F}$) species contribute to the resonance near 2 ppm, while the $Q^1{}_{1F}$ species contribute to the signal near -5 ppm. From our data there is no evidence for F-bonded $Q^{(2)}$ species.

While the dephasing of the $Q^0$ species appears virtually complete, Figure 8 illustrates further that only a minority of the $Q^{(1)}$ species are F-bonded. This result suggest that the $Q^1{}_{1F}$ species may have a somewhat lower stability than regular $Q^1$ species, disfavoring the modification reaction (2) relative to the others. Also, there is the possibility of F transfer reactions in the melt, such as $Q^1{}_{1F} + Q^0 \rightarrow Q^0{}_{1F} + Q^1$. The quantitative phosphate speciations illustrate further that only a fraction of the F species is engaging in this depolymerization reaction. This was already evident from Figure 2 and Table 2 which indicate that only about half or less of the fluorine species are P-bonded. As mentioned above this fraction is difficult to estimate quantitatively from the $^{19}F$ MAS NMR spectra as the relative intensities of the signals (acquired by rotor synchronized spin echoes) are compromised by differences in spin-spin relaxation rates. Assuming, however, that the back-projection procedure based on Figure 3b leads to similar correction factors in the other glasses, we can conclude that the fraction of F used for depolymerization of the phosphate network in the different samples lies between 37 and 62%, leading to a rough agreement between the <BO> contents deduced from the F speciations and those determined experimentally from $^{31}P$ MAS NMR. This comparison is illustrated in Table 4. In general, it indicates that in the $BiF_3$ containing glasses the fraction of fluoride ions participating in the depolymerization reactions (1)-(4) tends to be somewhat lower than in the $BiF_3$-free glasses. Towards the highest F contents the experimental <BO> values deviate substantially from those estimated from the fluoride ion speciations, indicating that the fraction of the fluoride species in effecting network depolymerization decreases with increasing F/P ratio. In part, this trend may also reflect larger amounts of F evaporation losses during the synthesis.

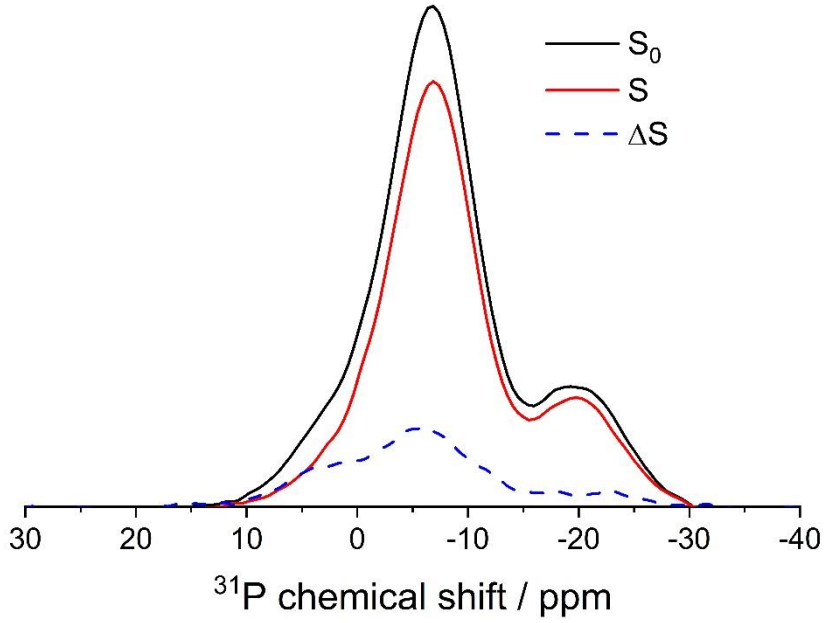


**Figure 8.** Fourier transforms of the signals $S_0$, $S$, and $\Delta S$, from the $^{31}P\{^{19}F\}$ REDOR data on a representative glass $y = 10$, for a dipolar mixing time of 100 µs.

**Table 4.** Average number of bridging oxygen atoms per phosphate species, <BO> measured experimentally and predicted from the fluorine speciation (listed are the fractions of P-bonded F species (±2%) deduced from the $^{19}F$ MAS NMR spectra).

| Glass | <BO>exp. | <BO>pred. | [$F_P$] |
|---|---|---|---|
| x = 0 | 1.39 | 1.51 | 55% |
| x = 2.5 | 1.24 | 1.26 | 59% |
| x = 5.0 | 1.12 | 1.00 | 58% |
| x = 7.5 | 1.04 | 0.60 | 60% |
| y = 5 | 1.32 | 1.23 | 62% |
| y = 10 | 1.20 | 1.10 | 55% |
| y = 20 | 1.07 | 0.75 | 49% |
| y = 30 | 0.98 | 0.61 | 37% |
| y = 40 | 0.84 | 0.00 | 38% |

**$^{23}$Na MAS single and double resonance NMR.**

The $^{23}$Na MAS NMR spectra are shown in Figure 9. A dominant resonance with a maximum near -10 ppm is observed for all the glass compositions. The lineshape shows the typical asymmetric form resulting from a wide distribution of quadrupolar coupling constants, affecting the signal of the central m = ½ <-> m = -½ transition of the quadrupolar $^{23}$Na nucleus as described by second-order perturbation theory.[45] The isotropic chemical shifts ($\delta_{iso}^{cs}$) extracted from Czjzek lineshape fits[38] are listed in Table 5; in addition the second-order quadrupolar effect (SOQE) values, defined by SOQE = $[C_Q^2(1 + \eta^2/3)]^{1/2}$ are given. Overall these data are consistent with a rather constant sodium environment.

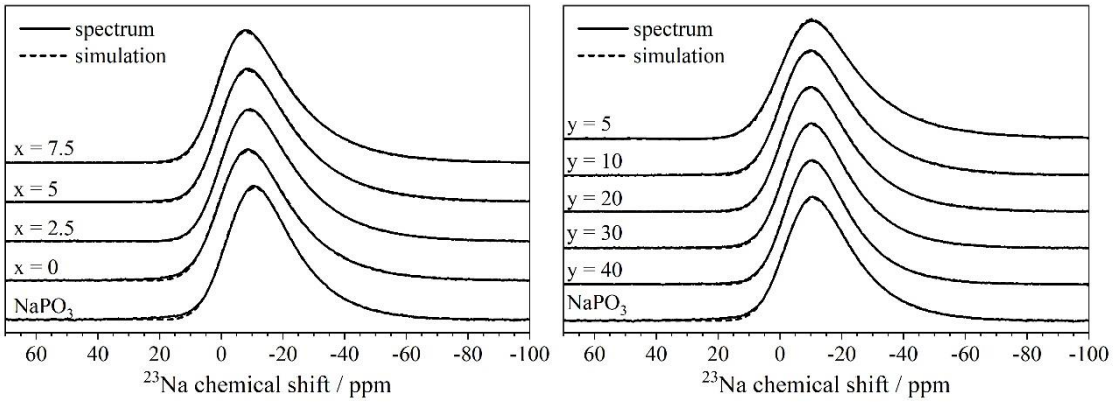


Figure 9. $^{23}$Na MAS NMR spectra of PFG-x and PFG-yBi glass series and vitreous $NaPO_3$.

The $^{23}$Na{$^{31}$P} REDOR results are shown in Figure 10, second moment values calibrated based on analogous data obtained on glassy $NaPO_3$ are included in Table 6. Although in the PFG-x system the P/Na ratio changes from 1.29 to 0.86, the second moment values remain virtually constant and are close to the value measured for glassy $NaPO_3$. This result suggests that the sodium ions dominantly interact with the phosphate rather than the fluoride species. In contrast, in the PFG-yBi series, the $M_{2(Na\text{-}P)}$ values are found to decrease significantly with increasing $BiF_3$ content even though the P/Na ratio remains constant (1.29) in this series. This dilution effect suggests an increasing participation of F in the first coordination sphere of the $^{23}$Na nuclei, which has also been confirmed by $^{23}$Na{$^{19}$F} REDOR experiments (data not shown). Overall, the effect is relatively small, however, suggesting that also in the Bi-containing glasses, the $Na^+$ ions also have a preference to associate with the phosphate, rather than the fluoride species.

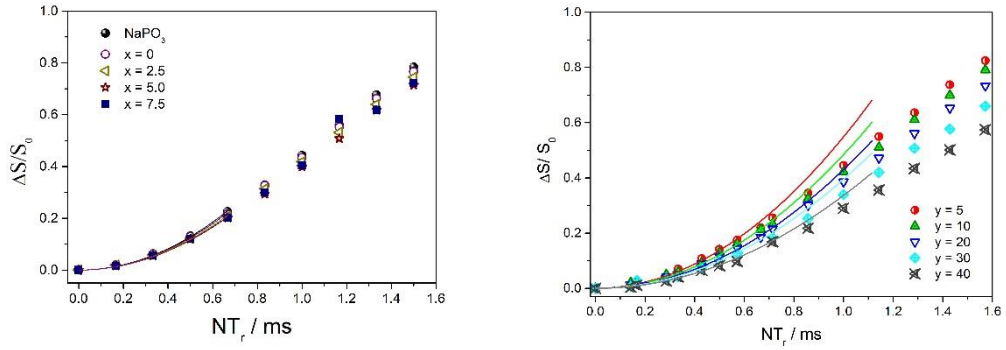


**Figure 10.** $^{23}$Na{$^{31}$P} REDOR dephasing curves of PFG-x and PFG-yBi glass series and vitreous $NaPO_3$.

**Table 5.** $^{23}$Na isotropic chemical shifts and SOQE parameters extracted from Czjzek fits[43] of the $^{23}$Na MAS NMR spectra and $M_{2(Na-P)}$ values measured via $^{23}$Na{$^{31}$P} REDOR. Values in parentheses were obtained by applying equation (1) to the experimental data before calibration with $NaPO_3$.

| Sample | $\delta_{iso}^{cs}$ (ppm) ±0.5 ppm | *SOQE* (MHz) ±0.2MHz | $M_{2(Na-P)}$ ($10^6$rad$^2$s$^{-2}$) ±10% |
|---|---|---|---|
| $NaPO_3$ | -1.8 | 2.3 | (3.8) 6.1 |
| x = 0 | 1.0 | 2.5 | (3.7) 5.9 |
| x = 2.5 | 0.7 | 2.5 | (3.6) 5.6 |
| x = 5.0 | 1.4 | 2.6 | (3.4) 5.5 |
| x = 7.5 | 2.0 | 2.6 | (3.4) 5.5 |
| y = 5 | 0.4 | 2.4 | (4.6) 6.5 |
| y = 10 | -0.1 | 2.5 | (3.9) 6.2 |
| y = 20 | -0.5 | 2.4 | (3.2) 5.2 |
| y = 30 | -1.3 | 2.3 | (2.9) 4.7 |
| y = 40 | -1.8 | 2.3 | (2.7) 4.4 |

# CONCLUSIONS

In conclusion, we have provided quantitative insights into the network organization and rare-earth coordination in bismuth fluorophosphate glass system. The results show that fluoride ions can serve as network modifiers in alkali/alkaline-earth phosphate glasses, leading to depolymerization of polyposphate chains and the formation of fluorophosphate network former units (NFU-s). NDU-s. However, only a fraction of the fluoride inventory

(50% or less) serves in this role, and this fraction is smaller in the $BiF_3$-containing glasses than in the Bi-free glasses. The $^{23}Na$ NMR and REDOR results suggest that sodium prefers interaction with phosphate rather than fluoride ions. A substantial amount of F is found within more clustered regions where they interact princially with the $Ba^{2+}$ and $Bi^{3+}$ ions.[18, 39, 40] While the local environment of Bi can, unfortunately, not be probed directly by $^{209}Bi$ NMR because of the strong nuclear electric quadrupole moment of the latter nucleus, the data of the present study suggest indirectly that the local environment of the $Bi^{3+}$ ions are dominated by fluoride rather than phosphate species. Possibly, new wideband detection techniques,[41] coupled with double resonance[42] may provide more quantitative insights into this issue in the future.

# ACKNOWLEDGMENTS

This research was conducted in the framework of the Photonics Quebec – Brazil Joint International Research Unit (SPEC-FAPESP funding process number 2015/22828-6) and the Brazilian agency Capes for financial support. GG and S.H. aknowledges funding by Fapesp, (grant number  and 2018/24735-3, respectively). H. E. and M. N. acknowledges funding by FAPESP, process number 2013/07793-6 (CEPID program). H. B. further gratefully acknowledges financial support from Deutsche Forschungsgemeinschaft.

# REFERENCES


(1) Maeder*, T. Review of Bi $_2$ O $_3$ Based Glasses for Electronics and Related Applications. *Int. Mater. Rev.* **2013**, *58* (1), 3–40. https://doi.org/10.1179/1743280412Y.0000000010.

(2) Romanov, A. N.; Haula, E. V.; Fattakhova, Z. T.; Veber, A. A.; Tsvetkov, V. B.; Zhigunov, D. M.; Korchak, V. N.; Sulimov, V. B. Near-IR Luminescence from Subvalent Bismuth Species in Fluoride Glass. *Opt. Mater. (Amst).* **2011**. https://doi.org/10.1016/j.optmat.2011.08.012.

(3) Ignat'eva, L. N.; Merkulov, E. B.; Stremousova, E. a.; Plotnichenko, V. G.; Koltashev, V. V.; Buznik, V. M. Effect of Bismuth Trifluoride on the Characteristics of Fluoroindate Glasses: The $InF_3$-$BiF_3$-$BaF_2$ System. *Russ. J. Inorg. Chem.* **2006**, *51* (10), 1641–1645. https://doi.org/10.1134/S0036023606100202.

(4) Romanov, A.; Fattakhova, Z.; Zhigunov, D.; Buchnev, L.; Korchak, V.; Sulimov, V. IR Luminescence from Subvalent Bismuth in Phosphate Glass and Glass-Ceramic Matrices: A New Insight into the Nature of Luminescent Bi Species. In *2011 Conference on Lasers and Electro-Optics Europe and 12th European Quantum Electronics Conference, CLEO EUROPE/EQEC 2011*; 2011. https://doi.org/10.1109/CLEOE.2011.5942831.

(5) Wang, L.; Tan, L.; Yue, Y.; Peng, M.; Qiu, J.; Mauro, J. Efficient Enhancement of Bismuth NIR Luminescence by Aluminum and Its Mechanism in Bismuth-Doped Germanate Laser Glass. *J. Am. Ceram. Soc.* **2016**. https://doi.org/10.1111/jace.14197.

(6) Liu, X.; Cheng, C.; Li, X.; Jiao, Q.; Dai, S. Controllable Ultra-Broadband Visible and near-Infrared Photoemissions in Bi-Doped Germanium-Borate Glasses. *J. Am. Ceram. Soc.* **2020**. https://doi.org/10.1111/jace.16721.

(7) Meng, X.; Qiu, J.; Peng, M.; Chen, D.; Zhao, Q.; Jiang, X.; Zhu, C. Infrared Broadband Emission of Bismuth-Doped Barium-Aluminum-Borate Glasses. *Opt. Express* **2005**, *13* (5), 1635. https://doi.org/10.1364/opex.13.001635.

(8) Dianov, E. M. Bismuth-Doped Optical Fibers: A Challenging Active Medium for near-IR Lasers and Optical Amplifiers. *Light Sci. Appl.* **2012**, *1* (MAY), 1–7. https://doi.org/10.1038/lsa.2012.12.

(9) Ding, J.; Zhao, G.; Tian, Y.; Chen, W.; Hu, L. Bismuth Silicate Glass: A New Choice for 2 Mm Fiber Lasers. *Opt. Mater. (Amst).* **2012**, *35* (1), 85–88. https://doi.org/10.1016/j.optmat.2012.07.003.

(10) Wei, X. T.; Zhao, J. B.; Chen, Y. H.; Yin, M.; Li, Y. Quantum Cutting Downconversion by Cooperative Energy Transfer from $Bi^{3+}$ to $Yb^{3+}$ in $Y_2O_3$ Phosphor. *Chinese Phys. B* **2010**, *19* (7). https://doi.org/10.1088/1674-1056/19/7/077804.

(11) Winterstein, A.; Manning, S.; Ebendorff-Heidepriem, H.; Wondraczek, L. Luminescence from Bismuth-Germanate Glasses and Its Manipulation through Oxidants. *Opt. Mater. Express* **2012**, *2* (10), 1320.

https://doi.org/10.1364/ome.2.001320.

(12) Bochentyn, B.; Warych, A.; Szreder, N.; Mielewczyk-Gryń, A.; Karczewski, J.; Prześniak-Welenc, M.; Gazda, M.; Kusz, B. Characterization of Structural, Thermal and Mechanical Properties of Bismuth Silicate Glasses. *J. Non. Cryst. Solids* **2016**, *439*, 51–56. https://doi.org/10.1016/j.jnoncrysol.2016.02.026.

(13) Gupta, G.; Sontakke, A. D.; Karmakar, P.; Biswas, K.; Balaji, S.; Saha, R.; Sen, R.; Annapurna, K. Influence of Bismuth on Structural, Elastic and Spectroscopic Properties of $Nd^{3+}$ Doped Zinc-Boro-Bismuthate Glasses. *J. Lumin.* **2014**, *149*, 163–169. https://doi.org/10.1016/j.jlumin.2014.01.032.

(14) Krishnan, M. L.; Neethish, M. M.; Ravi Kanth Kumar, V. V. Structural and Optical Studies of Rare Earth-Free Bismuth Silicate Glasses for White Light Generation. *J. Lumin.* **2018**. https://doi.org/10.1016/j.jlumin.2018.05.023.

(15) Ehrt, D. REVIEW: Phosphate and Fluoride Phosphate Optical Glasses — Properties, Structure and Applications. *Phys. Chem. Glas. Eur. J. Glas. Sci. Technol. Part B* **2015**, *56* (6), 217–234. https://doi.org/10.13036/17533562.56.6.217.

(16) Karmakar, B.; Kundu, P.; Dwivedi, R. N. UV Transparency and Structure of Fluorophosphate Glasses. *Mater. Lett.* **2002**, *57* (4), 953–958. https://doi.org/10.1016/S0167-577X(02)00903-5.

(17) Galleani, G.; Santagneli, S. H.; Messaddeq, Y.; De Oliveira, M.; Eckert, H. Rare-Earth Doped Fluoride Phosphate Glasses: Structural Foundations of Their Luminescence Properties. *Phys. Chem. Chem. Phys.* **2017**, *19* (32). https://doi.org/10.1039/c7cp03927a.

(18) Gonçalves, T. S.; Moreira Silva, R. J.; de Oliveira Junior, M.; Ferrari, C. R.; Poirier, G. Y.; Eckert, H.; de Camargo, A. S. S. Structure-Property Relations in New Fluorophosphate Glasses Singly- and Co-Doped with $Er^{3+}$ and $Yb^{3+}$. *Mater. Chem. Phys.* **2015**, *157*, 45–55. https://doi.org/10.1016/j.matchemphys.2015.03.012.

(19) Bradtmüller, H.; Zhang, L.; De Araujo, C. C.; Eckert, H.; Möncke, D.; Ehrt, D. Structural Studies of $NaPO_3$-$AlF_3$ Glasses by High-Resolution Double-Resonance Nuclear Magnetic Resonance Spectroscopy. *J. Phys. Chem. C* **2018**. https://doi.org/10.1021/acs.jpcc.8b06162.

(20) Zhang, X.; Zhang, R.; Hu, L.; Ren, J. Precipitation of $Er^{3+}$-Doped $Na_5Y_9F_{32}$ Crystals from Fluoro-Phosphate Glasses: An Advanced Solid-State NMR Spectroscopic Study. *J. Mater. Chem. C* **2019**, *7* (22), 6728–6743. https://doi.org/10.1039/c9tc00256a.

(21) Djouama, T.; Boutarfaia, A.; Poulain, M. Fluorophosphate Glasses Containing Manganese. *J. Phys. Chem. Solids* **2008**, *69* (11), 2756–2763. https://doi.org/10.1016/j.jpcs.2008.07.004.

(22) Galleani, G.; Doerenkamp, C.; Santagneli, S.; Magon, C. J.; De Camargo, A. S. S.; Eckert, H. Compositional Optimization of Emission Properties for Rare-Earth Doped Fluoride Phosphate Glasses: Structural Investigations via NMR, EPR, and Optical Spectroscopies. *J. Phys. Chem. C* **2019**, *123* (51), 31219–31231. https://doi.org/10.1021/acs.jpcc.9b10851.

(23) Bervas, M.; Badway, F.; Klein, L. C.; Amatucci, G. G. Bismuth Fluoride Nanocomposite as a Positive Electrode Material for Rechargeable Lithium Batteries. *Electrochem. Solid-State Lett.* **2005**. https://doi.org/10.1149/1.1861040.

(24) Gullion, T.; Schaefer, J. Rotational-Echo Double-Resonance NMR. *J. Magn. Reson.* **1989**, *81* (1), 196–200. https://doi.org/10.1007/1-4020-3910-7_89.

(25) Chan, J. C.; Eckert, H. Dipolar Coupling Information in Multispin Systems: Application of a Compensated REDOR NMR Approach to Inorganic Phosphates. Rotational Echo Double Resonance. *J. Magn. Reson.* **2000**, *147* (2), 170–178. https://doi.org/10.1006/jmre.2000.2191.

(26) Gullion, T. Measurement of Heteronuclear Dipolar Interactions by Rotational-Echo, Double-Resonance Nuclear Magnetic Resonance. *Magn. Reson. Rev.* **1997**.

(27) Duma, L.; Lai, W. C.; Carravetta, M.; Emsley, L.; Brown, S. P.; Levitt, M. H. Principles of Spin-Echo Modulation by J-Couplings in Magic-Angle-Spinning Solid-State NMR. *ChemPhysChem* **2004**. https://doi.org/10.1002/cphc.200301213.

(28) Massiot, D.; Fayon, F.; Capron, M.; King, I.; Le Calvé, S.; Alonso, B.; Durand, J. O.; Bujoli, B.; Gan, Z.; Hoatson, G. Modelling One- and Two-Dimensional Solid-State NMR Spectra. *Magn. Reson. Chem.* **2002**. https://doi.org/10.1002/mrc.984.

(29) Bertmer, M.; Eckert, H. Dephasing of Spin Echoes by Multiple Heteronuclear Dipolar Interactions in Rotational Echo Double Resonance NMR Experiments. *Solid State Nucl. Magn. Reson.* **1999**, *15* (3), 139–152. https://doi.org/10.1016/S0926-2040(99)00050-8.

(30) Van Vleck, J. H. The Dipolar Broadening of Magnetic Resonance Lines in Crystals. *Phys. Rev.* **1948**, *74* (9), 1168–1183. https://doi.org/10.1103/PhysRev.74.1168.

(31) Pemberton, J. E.; Latifzadeh, L.; Fletcher, J. P.; Risbud, S. H. Raman Spectroscopy of Calcium Phosphate Glasses with Varying CaO Modifier Concentrations. *Chem. Mater.* **1991**. https://doi.org/10.1021/cm00013a039.

(32) Brow, R.K., Tallant, D.R., Osborne, Z.A., Yang, Y., Day, D. E. Effect of Fluorine on the Structure of Phosphate Glass. *Phys. Chem. Glas.* **1991**, *32* (5), 188–195.

(33) Ignatieva, L. N.; Surovtsev, N. V.; Plotnichenko, V. G.; Koltachev, V. V.; Merkulov, E. B.; Polyshchuk, S. A.; Bouznik, V. M. The Peculiarities of Fluoride Glass Structure. Spectroscopic Study. *J. Non. Cryst. Solids* **2007**. https://doi.org/10.1016/j.jnoncrysol.2006.10.054.

(34) Bervas, M.; Badway, F.; Klein, L. C.; Amatucci, G. G.; Ignatieva, L. N.; Surovtsev, N. V.; Plotnichenko, V. G.; Koltachev, V. V.; Merkulov, E. B.; Polyshchuk, S. A.; et al. Structure and Ion Mobility in Glasses in the $BiF_3$-$PbF_2$-$ZrF_4$ Systems Studied by Raman and NMR Spectroscopy. *J. Non. Cryst. Solids* **2014**, *401* (4), 224–231. https://doi.org/10.1016/j.jnoncrysol.2014.01.028.

(35) Prescott, H. A.; Troyanov, S. I.; Kemnitz, E. The Synthesis and Crystal Structures of Two New Hydrated Sodium Monofluorophosphates: $NaHPO_3F \cdot$

2.5 $H_2O$ (I) and $Na_2PO_3F \cdot 10\ H_2O$ (II). *J. Solid State Chem.* **2001**. https://doi.org/10.1006/jssc.2000.9016.

(36) Zhang, L.; De Araujo, C. C.; Eckert, H. A New Sol-Gel Route to Aluminum Fluoride Phosphate Glasses: Mechanistic Investigations by NMR Spectroscopy. *Chem. Mater.* **2005**. https://doi.org/10.1021/cm050066z.

(37) Haubenreisser, U.; Sternberg, U.; Grimmer, A. R. High-Field $^{31}P$ N.M.R. Investigations of the Chemical Shielding and Indirect Dipolar Coupling of Polycrystalline Nuorophosphates. *Mol. Phys.* **1987**. https://doi.org/10.1080/00268978700100111.

(38) Espinose de Lacaillerie, J. B.; Fretigny, C.; Massiot, D. MAS NMR Spectra of Quadrupolar Nuclei in Disordered Solids: The Czjzek Model. *J. Magn. Reson.* **2008**. https://doi.org/10.1016/j.jmr.2008.03.001.

(39) de Oliveira, M.; Uesbeck, T.; Gonçalves, T. S.; Magon, C. J.; Pizani, P. S.; de Camargo, A. S. S.; Eckert, H. Network Structure and Rare-Earth Ion Local Environments in Fluoride Phosphate Photonic Glasses Studied by Solid-State NMR and Electron Paramagnetic Resonance Spectroscopies. *J. Phys. Chem. C* **2015**, *119* (43), 24574–24587. https://doi.org/10.1021/acs.jpcc.5b08088.

(40) de Oliveira, M.; Gonçalves, T. S.; Ferrari, C.; Magon, C. J.; Pizani, P. S.; de Camargo, A. S. S.; Eckert, H. Structure–Property Relations in Fluorophosphate Glasses: An Integrated Spectroscopic Strategy. *J. Phys. Chem. C* **2017**, *121* (5), 2968–2986. https://doi.org/10.1021/acs.jpcc.6b11405.

(41) O'Dell, L. A. The WURST Kind of Pulses in Solid-State NMR. *Solid State Nuclear Magnetic Resonance*. 2013. https://doi.org/10.1016/j.ssnmr.2013.10.003.

(42) Makrinich, M.; Nimerovsky, E.; Goldbourt, A. Pushing the Limit of NMR-Based Distance Measurements – Retrieving Dipolar Couplings to Spins with Extensively Large Quadrupolar Frequencies. *Solid State Nucl. Magn. Reson.* **2018**. https://doi.org/10.1016/j.ssnmr.2018.04.001.

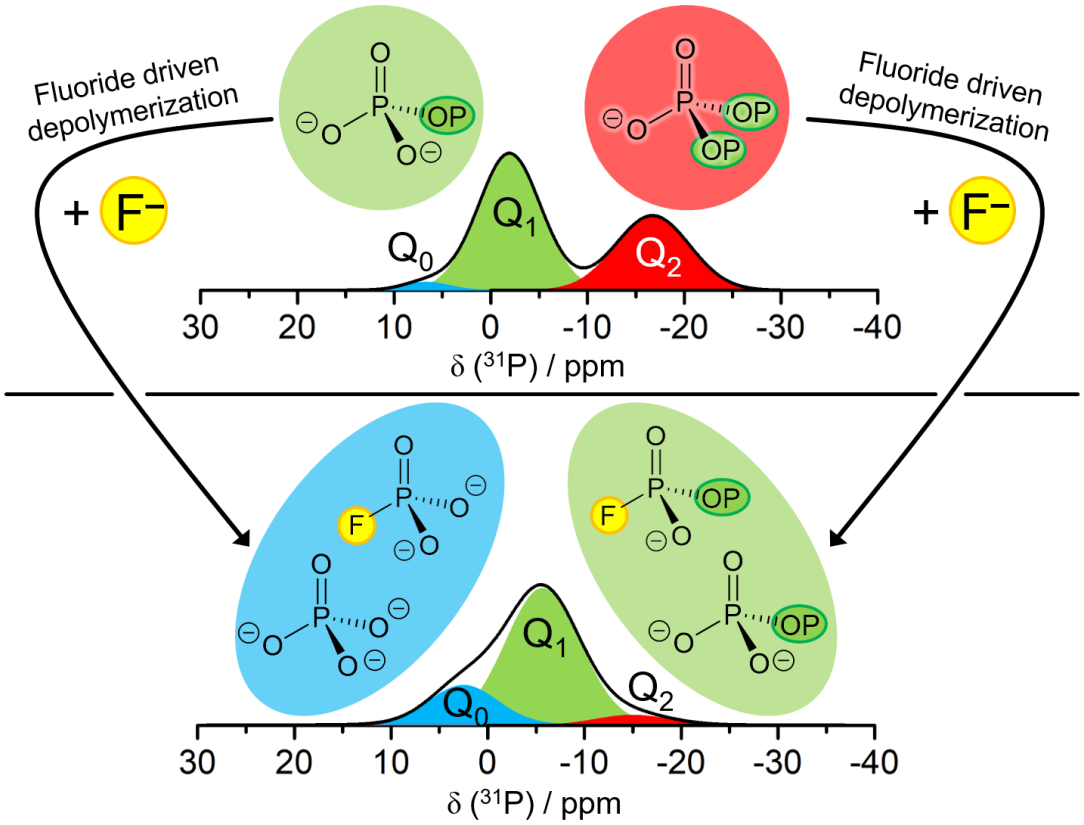
Fluoride driven depolymerization
+ F⁻
Fluoride driven depolymerization
+ F⁻
OP
OP
OP
Q0
Q1
Q2
30 20 10 0 -10 -20 -30 -40
δ (31P) / ppm
F
OP
OP
F
OP
Q0
Q1
Q2
30 20 10 0 -10 -20 -30 -40
δ (31P) / ppm